Oxidation of Carbon in Porous Solids

C. Y. Wen and S. C. Wang

Dept. of Chemical Engineering, West Virginia University
Morgantown, West Virginia

Noncatalytic solid-gas reaction systems are of great industrial importance and are found in daily use in chemical and metallurgical industries. Important examples are combustion of carbonaceous matters and regeneration of carbon-deposited catalysts by oxidation in air.

Weisz and Goodwin (7) observed, in the regeneration of catalysts at temperatures below 450°C, that the carbon burn-off is uniform (or "homogeneous") throughout the catalyst. At temperatures above 600°C, however, the burn-off is of "shell-progressive" or "unreacted-core-shrinking" type, as shown schematically in Figure 1.

Theoretical investigations have been undertaken previously to study the effect of heat and mass transfer processes on the overall rate of a noncatalytic solid-gas reaction occurring in a single solid pellet (4, 5, 8, 9). Phenomenological, rather than mechanistic, approach was adopted in analyzing these complex processes so that the effect of individual processes on the overall rate could be identified. The applicability and limitation of the "unreacted-core-shrinking" and "homogeneous" models were also presented, and the interrelationship between the two models was discussed. The concept of "effectiveness factor" frequently used in the studies of catalysis was extended to noncatalytic solid-gas reaction systems.

The purpose of the present experimental work is to verify the theoretical prediction of the existences of geometrical and thermal instabilities and the transition of the rate-controlling steps (ignition or extinction), which occur in a single particle-gas reaction describable by the unreacted-core-shrinking model.

Consider the simple case of solid-gas reaction taking place on the unreacted core surface:

$$aA(gas) + S(solid) \longrightarrow \text{Gas and/or Solid Product} \qquad (1)$$

The rate of reaction for gas component A, r_A, and for solid reactant S, r_S, can be represented as

$$r_A = a\, r_S = -\, a\, k_s\, C_S^m\, C_A^n$$

The above simplified rate equation will be used in view of the difficulty in obtaining a correct mechanism. As long as the rate equations fit the experimental data satisfactorily, the simple rate equations will provide an adequate analysis of overall characteristics of the reaction system provided no extrapolation beyond the range investigated is allowed.

Based on the unreacted-core-shrinking model as shown in Figure 1, and a constant particle size during an irreversible chemical reaction, a pseudo-steady-state material balance for the reactant component A within the inert solid product layer of the particle can be written as:

$$\nabla\cdot(CD_{eA}\,\nabla x_A) = (1/r^2)(\partial/\partial r)(r^2\, CD_{eA}\,\partial x_A/\partial r) = 0, \quad r_c < r < R$$

If the ideal-gas law holds for the gaseous phase, i.e., $C = P/\mathcal{R}T$, then at a constant total pressure P, $C \propto 1/T$. The effective diffusivity, D_{eA}, may be considered to be proportional to $T^{1.5\sim2.0}$ in the molecular diffusion regime, and to $T^{0.5}$ in the Knudsen diffusion regime. For convenience, D_{eA} may be taken to be roughly proportional to $T^{1.0}$ considering the possibility of both types of diffusion through the porous product layer. Therefore, the product CD_{eA} becomes proportional to T^0, that is temperature independent. It should be noted, however, that C or D_{eA} itself alone is affected by temperature variation. With these simplifications, the last equation now becomes

$$\frac{d^2x_A}{dr^2} + \frac{2}{r}\,\frac{dx_A}{dr} = 0 \qquad r_c < r < R \qquad (2)$$

The boundary conditions for Equation (2) are

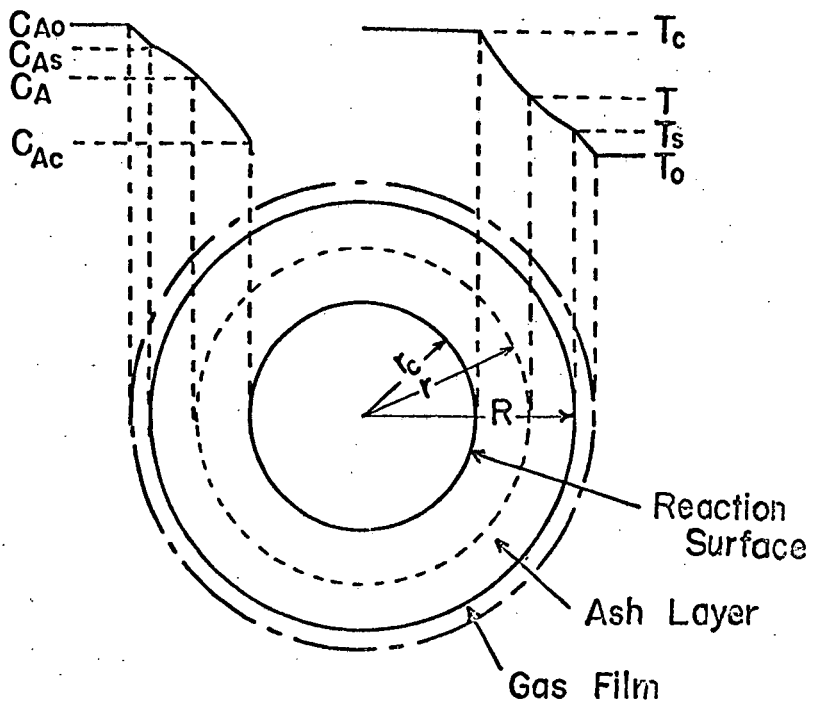

Fig. 1 Concentration and temperature profiles of a single particle–gas reaction indicating the three resistances in series.

$$r = R; \quad (CD_{eA})_{T_o} \left.\frac{dx_A}{dr}\right|_{r=R} = (k_{mA}C)_{T_o} \quad (x_{Ao} - x_{As}) \tag{3}$$

$$r = r_c; \ (CD_{eA})_{T_o} \left.\frac{dx_A}{dr}\right|_{r=r_c} = ak_{s(T_c)} \ C_{So}^m \ C_{Ac}^n \tag{4}$$

$$r = r_c; \ -(CD_{eA})_{T_o} \left.\frac{dx_A}{dr}\right|_{r=r_c} = aC_{So} \ \frac{dr_c}{dt} \tag{5}$$

where the subscripts T_o and T_c indicate the quantity to be evaluated at temperatures of bulk gas and reaction interface, respectively. The initial condition is

$$t = 0; \ r_c = R \tag{6}$$

For a particle with uniform distribution of solid reactant, the solid concentration, C_{So}, can be considered a constant at the surface of reaction, and therefore the reaction rate considered here is of the n-th order with respect to the concentration of gas component A.

Although equimolar counter-diffusion is assumed in deriving Equation (2), the application may be extended to non-equimolar cases when there is no significant volume change of gas or when concentrations of reactant and product gases are very dilute.

The heat balance in the ash layer is given by

$$\frac{\partial T}{\partial t} = \frac{k_e}{C_{pe}} \left(\frac{\partial^2 T}{\partial r^2} + \frac{2}{r} \frac{\partial T}{\partial r}\right) \qquad r_c < r < R \tag{7}$$

The boundary conditions are

$$r = R; \ -k_e \left.\frac{\partial T}{\partial r}\right|_{r=R} = h_C(T_s - T_o) + h_R \ (T_s^4 - T_w^4) \tag{8}$$

$$r=r_c; \ 4\pi r_c^2 ak_{s(T_c)} C_{So}^m C_{Ac}^n (-\Delta H) + 4\pi r_c^2 k_e \left.\frac{\partial T}{\partial r}\right|_{r=r_c} = \frac{4}{3}\pi r_c^3 \rho_c C_{pc} \frac{dT_c}{dt} \tag{9}$$

The initial condition is

$$t = 0; \ T = T_c = T_i \tag{10}$$

In Equation (9), it is assumed that the temperature within the unreacted core is uniform at T_c. The temperature dependency of the reaction rate constant is assumed to be of Arrhenius' type:

$$k_{s(T_c)} = k_s^o \exp(-E/\mathcal{R} T_c) \tag{11}$$

The effectiveness factor is defined as (4,5)

$$\eta_s = \frac{\text{Actual (overall) reaction rate}}{\text{Reaction rate obtainable when the reaction site is exposed to the gas concentration and temperature of the bulk gas phase}}$$

Thus,

$$\eta_s = \frac{4\pi r_c^2 ak_{s(T_c)} C_{So}^m C_{Ac}^n}{4\pi r_c^2 ak_{s(T_o)} C_{So}^m C_{Ao}^n} = \frac{k_{s(T_c)} C_{Ac}^n}{k_{s(T_o)} C_{Ao}^n} = \left(\frac{W_c}{U_c}\right)^n \exp\left[\frac{E}{\mathcal{R} T_o}\left(1 - \frac{1}{U_c}\right)\right] \tag{12}$$

or, by Equations (4) and (5),

$$\eta_s = -\frac{d\xi_c}{d\theta} \tag{13}$$

Equation (13) is true for all cases including those under isothermal situations.

Equations (2) through (10) are to be solved simultaneously by a numerical method. However, even for the simplest cases of pure heat transfer with moving

boundary, numerical methods are generally difficult and complicated. Therefore, some simplifying assumption seems warranted if there is no great sacrifice in accuracy in the final results. This can be accomplished by assuming $\partial T/\partial t = 0$ in Equation (7). However, such a pseudo-steady-state assumption could lead to errors as well as unreasonable instantaneous temperature changes (5,8,9). These situations can be compensated for by introducing a simple energy accumulation term into the heat balance equation for the ash layer. For this purpose, the temperature distribution in the ash layer can be approximated at all times by a steady state profile (1):

$$T = T_c + (T_s - T_c)\left(\frac{1}{r_c} - \frac{1}{r}\right) / \left(\frac{1}{r_c} - \frac{1}{R}\right) \tag{14}$$

The accumulation of energy in ash layer is

$$\text{acc.} = \int_{r_c}^{R} 4\pi C_{pe} r^2 \frac{\partial T}{\partial t}\, dr = 4\pi C_{pe}\left(\frac{d}{dt}\int_{r_c}^{R} r^2\, T\, dr + r_c^2 T_c \frac{dr_c}{dt}\right) \tag{15}$$

The integral in the last equation can now be evaluated using Equation (14). The accumulation in the ash layer can also be expressed as

$$\text{acc.} = -4\pi r_c^2 k_e \left.\frac{\partial T}{\partial r}\right|_{r=r_c} + 4\pi R^2 k_e \left.\frac{\partial T}{\partial r}\right|_{r=R} \tag{16}$$

The heat flux terms in Equation (16) can be obtained from Equations (8) and (9). Upon equating Equations (15) and (16) and simplifying, we obtain

$$a\, k_s(T_c) C_{So}^m C_{Ac}^n (-\Delta H)\, \xi_c^2 - [h_C(T_s - T_o) + h_R(T_s^4 - T_w^4)] = (R/3)(\rho_c C_{pc} - C_{pe})\, \xi_c^3 \frac{dT_c}{dt} +$$

$$(R/3) C_{pe} \frac{d}{dt}\left[T_c + (T_s - T_c) \cdot \frac{2 - 3\xi_c + \xi_c^3}{2(1-\xi_c)}\right] \tag{17}$$

With some additional mathematical manipulations, we obtain a final set of equations, Equations (17) through (23), which replace Equations (2) through (10).

$$\theta = 0; \quad \xi_c = 1 \tag{18}$$

$$\theta = 0; \quad U_c = U_i \tag{19}$$

$$W_c = W_s + N_{Sh}(1 - 1/\xi_c)(1 - W_s) \tag{20}$$

$$\frac{N_{Sh}(1-W_s)}{\phi_s \xi_c^2} = \left(\frac{W_c}{U_c}\right)^n \exp[(E/RT_o)(1 - 1/U_c)] = \eta_s \tag{21}$$

$$\frac{N_{Sh}(1-W_s)}{\phi_s \xi_c^2} = -\frac{d\xi_c}{d\theta} = \eta_s \tag{22}$$

$$U_s = U_c + (1 - 1/\xi_c)[(N_{Nu})_C (U_s - 1) + (N_{Nu})_R (U_s^4 - U_w^4)] \tag{23}$$

Equations (17) through (23) are a set of algebraic and ordinary differential equations, which can be solved easily by a numerical method.

When complete steady-state is assumed, there is no energy accumulation in the ash layer (A = 0) and in the unreacted core (G = 0). In this case it can be shown that Equations (17) through (23) reduce to

$$\eta_s = \frac{(N_{Nu})_C (U_s - 1) + (N_{Nu})_R (U_s^4 - U_w^4)}{\beta \phi_s (E/RT_o) \xi_c^2} \tag{24}$$

and

$$\frac{Y}{\beta\phi_s\left(\frac{E}{RT_o}\right)\xi_c^2} = \left[\frac{1-\frac{\frac{1}{N_{Sh}}+\frac{1}{\xi_c}-1}{(E/RT_o)\beta}\cdot Y}{U_s-\left(1-\frac{1}{\xi_c}\right)\cdot Y}\right]^n \cdot \exp\left[(E/RT_o)\left(1-\frac{1}{U_s-\left(1-\frac{1}{\xi_c}\right)\cdot Y}\right)\right] \qquad (25)$$

where $$Y = (N_{Nu})_C (U_s-1) + (N_{Nu})_R (U_s^4-U_w^4)$$

Existence of three roots for U_s at a fixed ξ_c is possible for equation (25).

Figures 2 and 3 show the plots of effectiveness factor vs. fractional solid reactant conversion, and compare unsteady-state heat transfer analysis to that of pseudo-steady-state. The solid lines in these figures are unsteady-state solutions of Equations (17)-(23) obtained by numerical method. The dashed and dotted lines represent stable and metastable solutions, respectively, of Equations (24) and (25) for the pseudo-steady-state case ($A = 0$, $G = 0$). Multiple solutions for η_s are possible for Equations (24) and (25) at a fixed X, as shown.

Figure 2 indicates a case in which the pseudo-steady-state analysis could lead to an erroneous conclusion. The chemical-reaction-controlling region would have never been realized if the pseudo-steady-state analysis had been used. The unsteady-state analysis on the other hand shows that chemical reaction could be rate-controlling when the initial temperature of the particle is sufficiently low ($U_i = 0.90$). Figure 3 depicts the effect of heat capacity of unreacted core and heat of reaction on the thermal instability. The occurrence of thermal instability is less likely when the heat capacity is high.

Figure 4 illustrates an example of experimental result, which is computed based on the unreacted-core-shrinking model. The corresponding solutions obtained from Equations (17)-(23) (solid line) and from Equations (24) and (25) (dashed and dotted lines) are also shown in the figure for comparison. The experiment was performed in a thermobalance by burning a single solid sphere in a stream of heated air. The solid pellet was prepared by mixing a desired proportion of activated charcoal with aluminum oxide that serves as an inert porous medium. Waterglass (sodium silicate) diluted with a proper amount of water was used as a binder in forming the pellets. The particle was heated at 700°C in an inert atmosphere prior to the combustion test to remove moisture and to insure no weight loss owing to inert solid during the test. "Extinction" occurred at about 85 percent of solid conversion. The unsteady-state heat transfer analysis (solid line) describes more closely the experimental result than the pseudo-steady-state (dashed line) at the initial stage and during the transition from diffusion- to chemical-reaction-controlled regime. The values of effective diffusivity (6) and effective thermal conductivity (3) are estimated based on empirical correlations. The activation energy and surface rate constant are calculated from a correlation obtained by Field, et.al (2) based on data of various investigators. In view of the wide variety of data reported in the literature for the oxidation of carbon, these values are believed to be good estimates for this purpose. The point to be emphasized here is that it is possible to predict the approximate reaction path of a solid-gas reaction from the estimated values of physical and chemical properties.

In general, it was found that most of the characteristic behavior from theoretical predictions are verifiable by the experimental observation. The phenomena of geometrical and thermal instabilities of reacting solid are experimentally verified. The reaction path is easily followed by plotting the effectiveness factor (or rate per unit area of reaction interface) versus solid conversion. Ignition and extinction are also observed under certain conditions agreeing, at least qualitatively, with the theory.

NOTATIONS

a stoichiometric coefficient

A $C_{Ao} D_{eA(T_o)} C_{pc}/aC_{So}k_e$

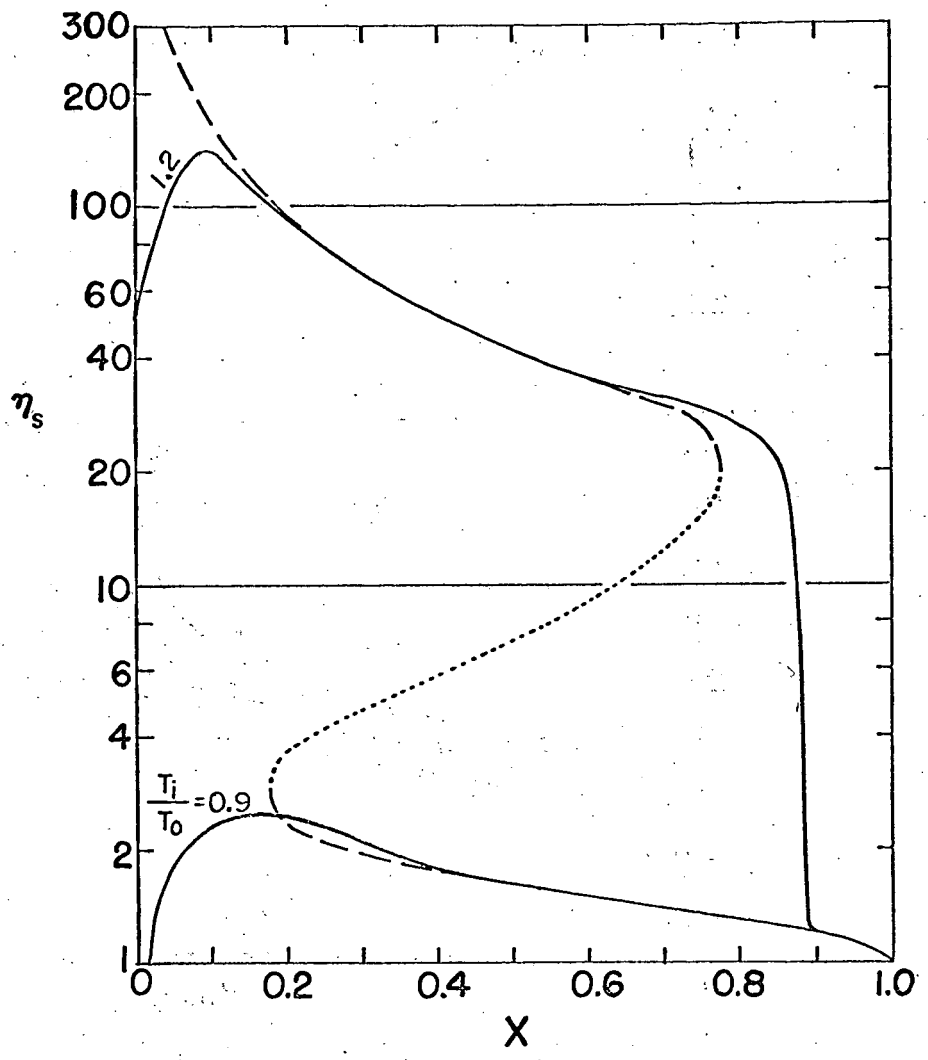

$\beta = 0.005$ $\quad \phi_s = 0.139$ $\quad A = 0$

$N_{Sh} = 100$ $\quad (N_{Nu})_C = 1$ $\quad (N_{Nu})_R = 0$

$\frac{E}{\mathcal{R} T_o} = 25$ $\quad n = 1$ $\quad G = 0.5$

Fig.2 An Example Showing the Difference between Steady and Unsteady State Analysis

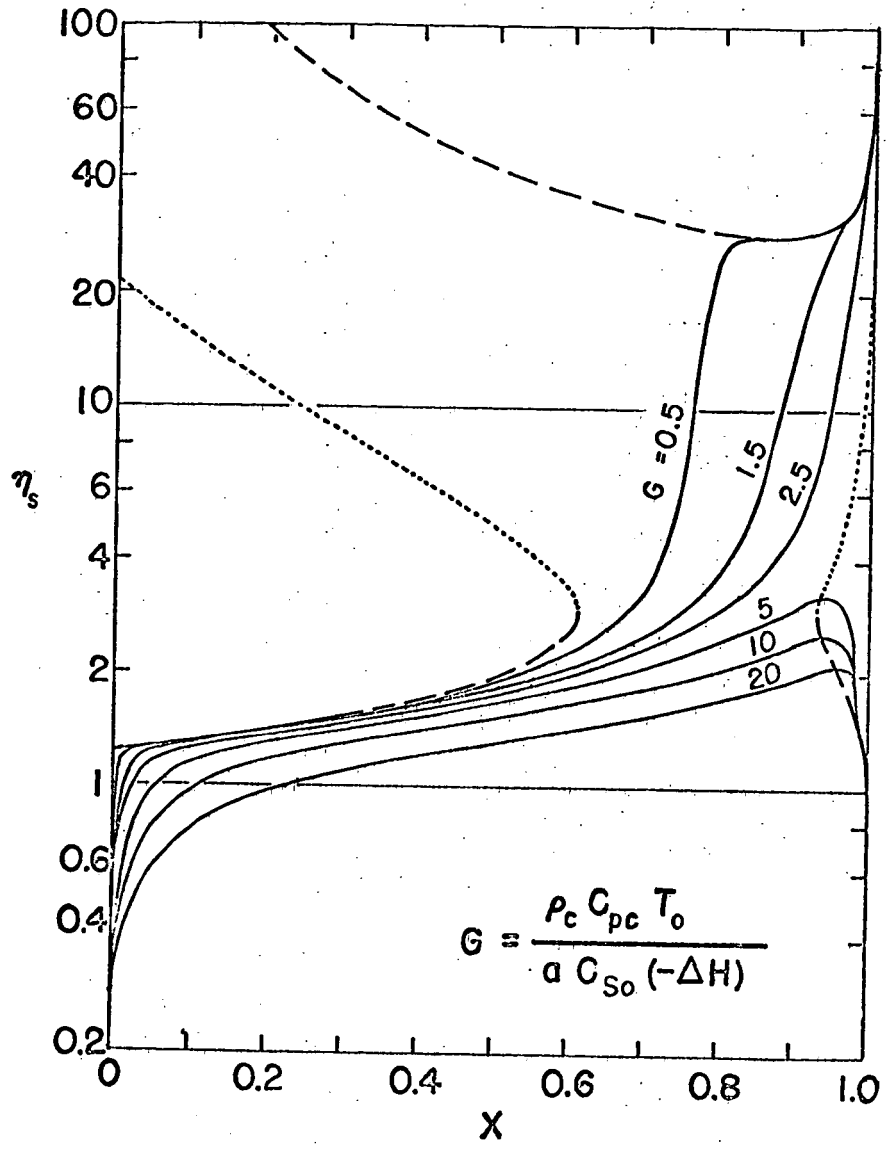

$\beta = 0.02$ $\quad \phi_s = 0.139$ $\quad A = 0$

$N_{Sh} = 100$ $\quad (N_{Nu})_C = 10$ $\quad (N_{Nu})_R = 0$

$\frac{E}{\mathcal{R} T_o} = 25$ $\quad n = 1$ $\quad \frac{T_i}{T_o} = 0.95$

Fig.3 The Effect of Heat of Reaction and Heat Capacity of Unreacted Core on Thermal Instability in Terms of G.

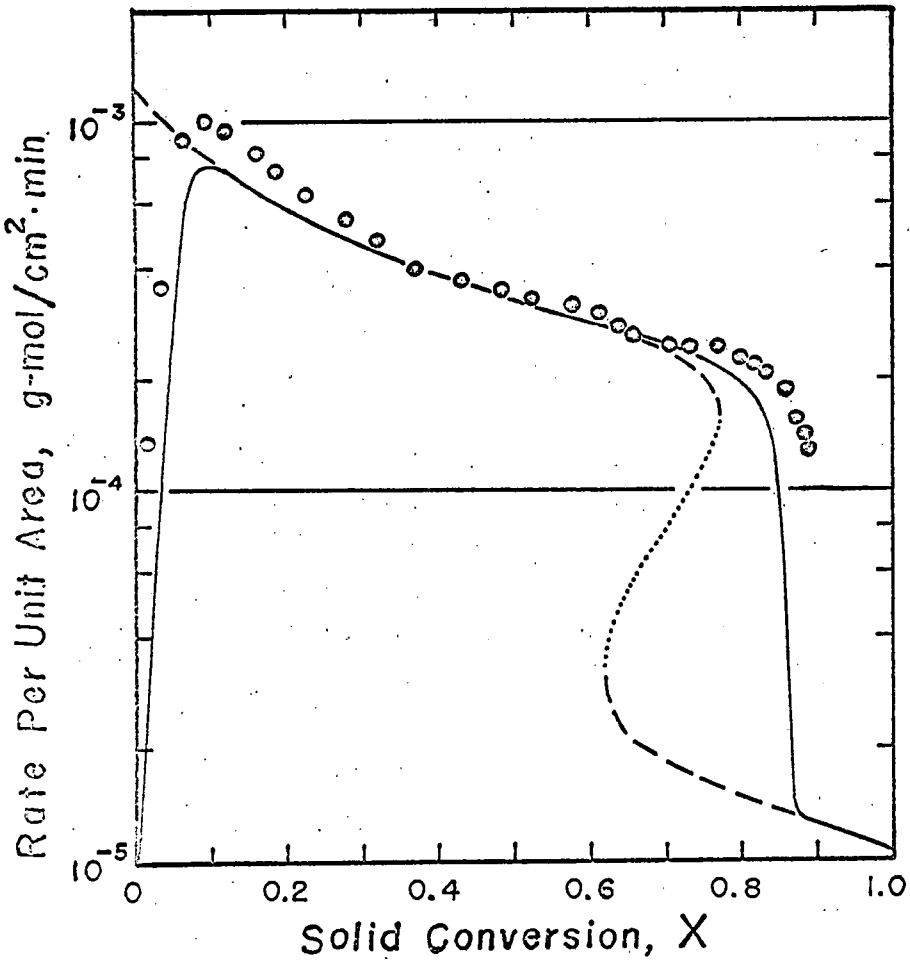

T_o = 442 °C
T_w = 573 °C
T_i = 27 °C
N_{Re} = 393
R = 1.244 cm
C_{So} = 0.0225 g-mol/cm^3
ε = 0.556
D_{eA} = 0.321 cm^2/sec
k_e = 0.0032 cal/sec·cm·°C
E = 35,700 cal/g-mol
$k_{s(T_o)}$ = 5.16 x 10^{-4} cm/sec

Fig.4 Comparison of Experimental Result and Computer Simulation for Oxidation of Carbon in Porous Solid, Using Unreacted-Core-Shrinking Model

C	total concentration of gases, mole/L^3
C_A	concentration of species A, C_{Ac} at unreacted-core surface, C_{Ao} in bulk gas phase, C_{As} at outer surface of particle, mole/L^3
C_S	concentration of solid reactant S, C_{So} initial concentration, mole/L^3
C_{pc}	heat capacity of unreacted core, H/MT
C_{pe}	volumetric heat capacity of ash layer, H/L^3T
D_{eA}	effective diffusivity of gaseous component A in ash layer, L^2/θ
E	activation energy of reaction rate constant, H/mole
G	$\rho_c C_{pc} T_o / a C_{So}(-\Delta H)$, ratio of enthalpy of unreacted core to heat of reaction
h_C	convective heat transfer coefficient, H/$L^2\theta$ T
h_R	radiational heat transfer coefficient, H/$L^2\theta T^4$
ΔH	heat of reaction per mole of gaseous reactant, H/mole
k_e	effective thermal conductivity of ash layer, H/Lθ T
k_{mA}	mass transfer coefficient of component A across gas film, L/θ
k_s	surface reaction rate constant based on solid reactant, $L^{3(m+n)-2}/mole^{m+n-1}\theta$
k_s^o	frequency factor for rate constant, $L^{3(m+n)-2}/mole^{m+n-1}\theta$
m	order of reaction for solid reactant
n	order of reaction for gaseous reactant
$(N_{Nu})_C$	Rh_C/k_e, modified Nusselt number for convective heat transfer
$(N_{Nu})_R$	$Rh_R T_o^3/k_e$, modified Nusselt number for radiational heat transfer
N_{Re}	particle Reynolds number
N_{Sh}	$Rk_{mA(T_o)}/D_{eA(T_o)}$, modified Sherwood number
P	total pressure, F/L^2
r	distance from center of sphere, L
r_c	radius of unreacted core, L
r_A, r_S	surface reaction rates of gaseous reactant A and solid reactant S, respectively, mole/$L^2\theta$
R	particle radius, L
$\mathcal{R}$	gas constant, H/mole.T
t	time, θ
T	temperature, T_c at unreacted-core surface, T_i initial temperature of particle, T_o at bulk gas phase, T_s at outer surface of particle, T_w at reactor wall, T
U	T/T_o
U_c	T_c/T_o
U_i	T_i/T_o
U_s	T_s/T_o
U_w	T_w/T_o
W	x_A/x_{Ao}, $W_c = x_{Ac}/x_{Ao}$, $W_s = x_{As}/x_{Ao}$
x_A	mole fraction of component A, x_{Ac} at unreacted-core surface, x_{Ao} in bulk gas phase, x_{As} at outer surface of particle
X	$1 - \xi_c^3$, fractional conversion of solid reactant S
β	$C_{Ao} D_{eA(T_o)}(-\Delta H)\mathcal{R}/k_e E$
ϵ	porosity of ash layer

η_s effectiveness factor

θ $k_{s(T_o)} C_{Ao}^{n} C_{So}^{m-1} t/R$

ξ r/R

ξ_c r_c/R

ρ_c density of unreacted core, M/L^3

ϕ_s $aRk_{s(T_o)} C_{Ao}^{n-1} C_{So}^{m} / D_{eA(T_o)}$

LITERATURE CITED

1. Beveridge, G. S. G., and Goldie, P. J., Chem. Eng. Sci., 23, 913 (1968).
2. Field, M. A., Gill, D. W., Morgan, B. B. and Hawksley, P. G. W., COMBUSTION OF PULVERISED COAL, The British Coal Utilisation Research Association, Leatherhead, Surrey, England (1967).
3. Francl, J. and Kingery, W. D., Am. Ceramic Soc. Journal, 37, 99 (1954).
4. Ishida, M. and Wen, C. Y., A.I.Ch.E. Journal, 14, 311 (1968).
5. Ishida, M. and Wen, C. Y., Chem. Eng. Sci., 23, 125 (1968).
6. Satterfield, C. N. and Sherwood, T. K., THE ROLE OF DIFFUSION IN CATALYSIS, Addison-Wesley, Reading, Mass. (1963).
7. Weisz, P. B. and Goodwin, R. D., J. Catalysis, 2, 397 (1963).
8. Wen, C. Y., Ind. Eng. Chem., 60, No. 9, 34 (1968).
9. Wen, C. Y., and Wang, S. C., "Thermal and Diffusional Effects in Noncatalytic Solid Gas Reactions", to appear in Ind. Eng. Chem., July, 1970 issue.